

Thermal drawdown-induced flow channeling in a single fracture in EGS



Bin Guo^{a,b}, Pengcheng Fu^{a,*}, Yue Hao^a, Catherine A. Peters^b, Charles R. Carrigan^a

^a Atmospheric, Earth and Energy Division, Lawrence Livermore National Laboratory, United States

^b Department of Civil and Environmental Engineering, Princeton University, United States

ARTICLE INFO

Article history:

Received 9 June 2015

Received in revised form

11 November 2015

Accepted 10 January 2016

Available online 28 January 2016

Keywords:

EGS

Thermal drawdown

Flow channeling

Aperture heterogeneity

THM coupling

GEOS

ABSTRACT

The evolution of flow pattern along a single fracture and its effects on heat production is a fundamental problem in the assessments of engineered geothermal systems (EGS). The channelized flow pattern associated with ubiquitous heterogeneity in fracture aperture distribution causes non-uniform temperature decrease in the rock body, which makes the flow increasingly concentrated into some preferential paths through the action of thermal stress. This mechanism may cause rapid heat production deterioration of EGS reservoirs. In this study, we investigated the effects of aperture heterogeneity on flow pattern evolution in a single fracture in a low-permeability crystalline formation. We developed a numerical model on the platform of GEOS to simulate the coupled thermo-hydro-mechanical processes in a penny-shaped fracture accessed via an injection well and a production well. We find that aperture heterogeneity generally exacerbates flow channeling and reservoir performance generally decreases with longer correlation length of aperture field. The expected production life is highly variable (5 years to beyond 30 years) when the aperture correlation length is longer than 1/5 of the well distance, whereas a homogeneous fracture behaves similar to a homogeneous one when the correlation length is much shorter than the well distance. Besides, the mean production life decreases with greater aperture standard deviation only when the correlation length is relatively long. Although flow channeling is inevitable, initial aperture fields and well locations that enable tortuous preferential paths tend to deliver long heat production lives.

© 2016 The Authors. Published by Elsevier Ltd. This is an open access article under the CC BY-NC-ND license (<http://creativecommons.org/licenses/by-nc-nd/4.0/>).

1. Introduction

Engineered (or enhanced) geothermal systems (EGS) are promising energy resources with an enormous potential for base-load electricity generation (Tester et al., 2006; Lund et al., 2011; Bertani, 2012; Jung, 2013). Unlike conventional hydrothermal energy, EGS is not limited to locations with abundant water supply and high-conductivity formations. Engineering measures such as hydraulic fracturing and hydraulic shearing provide the opportunity to extract heat from originally low-permeability crystalline formations by creating new fractures and/or enhancing the permeabilities of natural fractures (Brown and Duchane, 1999; Tenma et al., 2008; Brown, 2009). Water circulation in an EGS reservoir can be dominated by flow in a single fracture/fault (Brown, 1997; Brown and Duchane, 1999; Chopra and Wyborn, 2003; Baisch et al., 2006; Brown, 2009; Llanos et al., 2015) or through an interconnected fracture network (Koh et al., 2011; Genter et al., 2012, 2013).

In either case, the flow pattern as well as its evolution along an individual fracture and the heat exchange between the working fluid and the rock surrounding this fracture play a fundamental role in heat production.

Fluid flow and heat exchange closely interact during EGS heat production. Because heat is transferred from the rock surrounding the fracture to the production well(s) by flowing fluid, only the portion of fracture that carries flow provides effective heat exchange surface area. It is therefore highly desirable to have flow spreading over a large area of the fracture surface. However, spatially heterogeneous fractures are ubiquitous in geologic formations (Neretnieks, 1987; Méheust and Schmittbuhl, 2000; Kosakowski et al., 2001) and fluid flow in a fracture with aperture heterogeneity tends to be channelized along a few preferential paths (Tsang and Tsang, 1989). The rock body near the preferential paths tends to cool faster than other regions do, and the cooled rock body develops thermal stress that reduces the effective compressive stress acting on the preferential flow paths and thereby increases the fracture aperture. The increase of aperture, in turn, makes the flow even more channelized along these preferential paths. In the present study, the term “flow channeling” refers

* Corresponding author at: 7000 East Avenue, Livermore, CA 94550, United States.
E-mail address: fu4@llnl.gov (P. Fu).

to the phenomenon or process of the preferential paths carrying an increasing portion of the flow. This mechanism is expected to reduce heat exchange efficiency and cause rapid heat production deterioration.

Numerous studies have shown evidence for fracture aperture/transmissivity evolution due to the thermo-hydro-mechanical (THM) processes in EGS reservoirs dominated by either a single fracture/fault or a fracture network (Kolditz and Clauser, 1998; Parker, 1999; Tenma et al., 2008). For example, Bower and Zvoloski (1997) coupled stress to a flow and heat transfer model and found that the fracture flow increases due to further opening of a single fracture in the Fenton Hill hot dry rock reservoir. Danko and Bahrami (2012) used a THM model to simulate the heat production in two EGS reservoirs at Fenton Hill and Desert Peak, each of which was modeled to be dominated by a single fracture. They observed that only the aperture near the central part of the fracture increases over time. Hicks et al. (1996) simulated the THM processes in a fractured rock and observed a decreasing injection pressure and an increasing water recovery percentage, indicating an increase in the overall permeability. Koh et al. (2011) also found great enhancement of injectivity at a given pressure drop over 10 years in naturally fractured rock. Fu et al. (2015) conducted THM coupled simulations of heat production in fracture networks and observed that the flow inevitably becomes more concentrated into a few channels during heat production. Although THM processes significantly affects heat production in those studies, the quantitative effects of spatially heterogeneous fracture aperture on flow channeling remains poorly understood.

A number of studies, such as Taron and Elsworth (2009), Pandey et al. (2014), Ameli et al. (2014), Deng et al. (2015), etc. have shown that geochemical reactions could alter permeability/transmissivity of fractures and porous media under certain conditions. However, the current study focuses on THM processes and does not consider geochemistry for two reasons: First, quartz, the main component of crystalline rocks (the host formations of most EGS), reacts with water very slowly and the effects of water-quartz reaction on aperture alteration are expected to be negligible within the typical lifespan of EGS. Second, the THM process investigated herein alone can have very significant effects on EGS performance and it is more appropriate to study the effects of geochemistry in separate work.

The present study develops a numerical model that fully couples the THM processes during heat production and quantitatively investigates the effects of spatial heterogeneity in aperture on flow channeling in a single planar fracture in an EGS reservoir. We especially focus on how the probability distribution and spatial autocorrelation characteristics of the aperture field affect the reservoir performance. The results are directly useful for EGS reservoirs dominated by a single fracture/fault, and they also provide useful insights into the fundamental behavior of individual fractures in a fracture network.

2. Coupled THM model

2.1. Overview of the model

We developed a new numerical model on GEOS, a high performance computing (HPC) platform developed at the Lawrence Livermore National Laboratory (LLNL) (Fu and Carrigan, 2012; Settigast et al., 2012; Fu et al., 2013), to simulate the coupled THM processes in the heat production stage of an EGS reservoir. The essential processes/mechanisms (Pruess, 1990; Hayashi et al., 1999; McDermott et al., 2006; Guo et al., 2015) involved in the flow channeling phenomenon include:

1. Fluid flow along a fracture and in the rock matrix, as well as its evolution as the aperture/permeability field changes;
2. Convective heat transfer associated with the fluid flow along the fracture, conductive heat transfer in the rock matrix, and heat exchange between the working fluid and the surrounding rock body;
3. The change of total stress caused by the non-uniform cooling of the rock body; and
4. The evolution of the local fracture aperture as the effective stress changes.

The first two processes are simulated by a combined flow and heat transfer solver developed in GEOS, as shown in Fig. 1 and elaborated on in Section 2.2. Thermal stress is calculated by a thermo-mechanical solver and the total stress tensor of each rock matrix element is updated accordingly as briefly described in Section 2.3. Section 2.4 presents the procedure of updating the fracture aperture field based on the fluid pressure and stress change along the fracture in the reservoir.

2.2. Flow and heat transfer in fracture and matrix

The flow and heat transfer solver combines fluid flow and heat transfer in both fractures and rock matrix. We use a finite volume formulation to solve the independent state variables, namely fluid pressure P and temperature T , for 3D 8-node hexahedron elements. The coupled single-phase flow and heat transfer in porous medium are governed by the principle of mass and energy conservation. The mass conservation equation for compressible fluid is

$$\frac{\partial(\rho\phi)}{\partial t} + \nabla \cdot (\rho\mathbf{v}) = \Gamma \quad (1),$$

where ρ is the fluid density; ϕ is the rock porosity; t is time; \mathbf{v} is the fluid velocity vector; and Γ is a source/sink term. According to Darcy's law, fluid velocity vector v is calculated as

$$\mathbf{v} = -\frac{\mathbf{k}}{\mu}(\nabla P - \rho\mathbf{g}) \quad (2),$$

where \mathbf{k} is the intrinsic permeability tensor of the rock matrix; μ is the fluid dynamic viscosity; and \mathbf{g} is the gravity acceleration vector. The current study assumes the permeability of rock matrix to be isotropic, so the permeability tensor is reduced to the permeability scalar k . Substituting Eq. (2) into Eq. (1) yields

$$\frac{\partial(\rho\phi)}{\partial t} - \nabla \cdot \left[\rho \frac{k}{\mu} (\nabla P - \rho\mathbf{g}) \right] = \Gamma \quad (3).$$

Fluid density ρ depends on fluid pressure and temperature, as approximated by the following analytical function

$$\rho = \rho_r e^{[\beta_f(P-P_r) + \alpha_f(T-T_r)]} \quad (4),$$

where ρ_r , P_r , T_r , β_f , and α_f are the fluid density, pressure, temperature, fluid compressibility, and fluid thermal expansion coefficient, respectively, in a known reference state.

The fracture, while hydraulically conductive, is mechanically closed under the high *in situ* compressive stress assumed in this study. GEOS has the capability to represent fractures using planar "face element" embedded in the solid mesh as described in Guo et al. (2015). However this treatment is computational expensive and is unnecessary for the current study due to the simple geometry that we investigate. The fracture in the present model is represented by a very thin layer (2 mm thick) of porous medium. When Eq. (3) is applied to fracture grid elements, the porosity is set as unity and the effective permeability k_f is calculated according to the cubic law (Berkowitz, 2002) as

$$k_f = \frac{A^3}{12H} \quad (5),$$

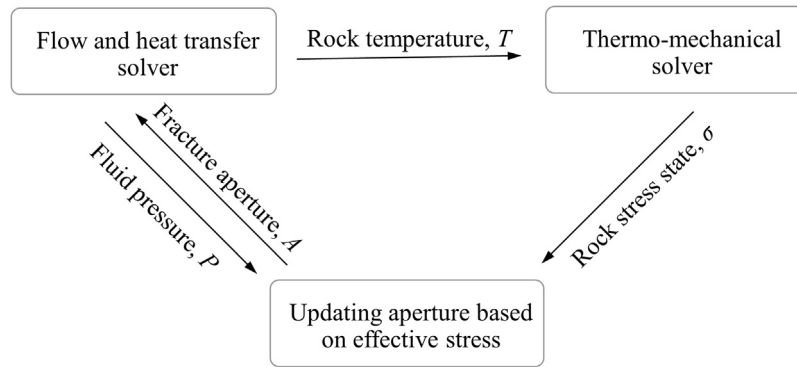


Fig. 1. Coupling of flow, heat transfer, and thermo-mechanical processes in the model.

where A is the fracture aperture; and H is the thickness of the fracture grid elements in the mesh. At each point, fracture aperture depends on the effective stress normal to the fracture plane. Spatially, aperture is treated as an auto-correlated random field across the fracture plane. Section 2.4 and Section 3.2 elaborate on these two aspects, respectively.

The governing equation describing the energy balance over the fluid phase and the solid phase in a porous medium is

$$\frac{\partial}{\partial t} (\phi \rho C_f T + (1 - \phi) \rho_s C_s T) + \nabla \cdot (\rho C_f \mathbf{T} \mathbf{v}) = \nabla \cdot (K_m \nabla T) + Q \quad (6),$$

where C_f is the specific heat capacity of the fluid; ρ_s is the rock solid density; C_s is the specific heat capacity of the rock solid; K_m is the thermal conductivity of the rock matrix; and Q is a source/sink term of heat.

We use an implicit time integration scheme in the flow solver and the time step size is adaptively adjusted. Generally, small time steps are required in the beginning of the heat production due to the high degree of transience of the system. As the system evolves into a semi-steady state, relatively long time steps suffice. Because the apertures in the fracture are assumed to remain constant within each time step, we limit the time step size to be no longer than one month. A sensitivity study found that further reducing this maximum time step size does not alter the simulation results, confirming sufficient temporal resolution.

2.3. Calculation of thermal stress

The rock body containing the closed fracture is treated as a continuum for the calculation of thermal stress. The mesh is the same as that for the flow and heat transfer solver. The thermal stress field is obtained following the procedure outlined in Section 2.10 of Cook et al. (2007). The approach is a standard method employed in thermo-mechanical finite element analysis and not repeated here.

2.4. Updating the fracture aperture field

To evolve the apertures of the fracture during heat production requires: (1) total stress in the rock medium surrounding the fracture plane, (2) the fluid pressure field in the fracture, and (3) a rock joint model. The total stress tensor of the rock body, including the contributions of the far-field *in situ* stress and the thermal stress, is a direct output of the thermo-mechanical solver. The fluid pressure is obtained from the flow and heat transfer solver, and the difference between the total normal stress and the fluid pressure is the effective normal stress σ'_n of the fracture element. We assume that the aperture of each fracture element is solely determined by the effective normal stress on this element and use the classic Barton–Bandis model (Bandis et al., 1983; Barton et al., 1986) to calculate the aperture.

The Barton–Bandis model for rock joints has been widely used in various numerical models for fracture-dominated geothermal reservoirs (e.g., Kohl et al., 1995; Bower and Zyvoloski, 1997; Bruel, 2002). We rewrite the original equation to express aperture as a function of effective stress as

$$A = A_{\max} - \frac{a\sigma'_n}{1 + b\sigma'_n} \quad (7),$$

where A is the aperture under the current effective normal stress σ'_n , and A_{\max} is the aperture at zero (or a minimal) effective stress. a and b are two material- and state-dependent parameters. We assume that the aperture diminishes to zero as the effective stress approaches infinity so that the relationship of $A_{\max} = a/b$ reduces the independent parameters to a and b alone. Essentially, a random field of fracture aperture (including its current state and its evolution with respect to stress) can be fully represented by the fields of a and b . Studies in the literature either focused on the relationship between aperture and stress for a fracture of a small “representative area” (Bandis et al., 1983; Barton et al., 1985) or quantified the aperture’s spatial distribution at a specific stress state (Cook, 1992; Bower and Zyvoloski, 1997; Auradou et al., 2006; Danko and Bahrami, 2012; Llanos et al., 2015). However, the current study needs to capture both aspects and we achieve this through the method described in Section 3.2.

3. Model setup

3.1. Simulation domain and boundary conditions

We simulate the heat production from a horizontal penny-shaped fracture in a large body of low-permeability hot crystalline rock. The system somewhat resembles the Habanero project in the Cooper Basin, Australia (Chopra and Wyborn, 2003; Baisch et al., 2009; Llanos et al., 2015), but this study is not aimed at this specific EGS site. The diameter of the fracture is 1,000 m at a depth of 3,000 m. One injection well and one production well intersect the fracture and the distance between the two wells is 500 m. Fig. 2 shows the system geometry as well as the three principal components of the *in situ* stress at the depth of the fracture. The site is in a reverse faulting region according to Anderson’s classification (Anderson, 1951) with the vertical stress being the minimum principal component. Therefore, the horizontal fracture can be a hydraulic fracture (McClure and Horne, 2014) or a natural fracture. As we explicitly quantify the spatial heterogeneity of aperture field, the geological origin of the fracture does not directly affect the current study. The initial pore pressure is 34 MPa at the fracture depth, and we ensure that the fluid pressure never exceeds the minimum principal stress during heat production, so the extent of the fracture remains constant. The initial rock temperature is 200 °C (392 °F) at

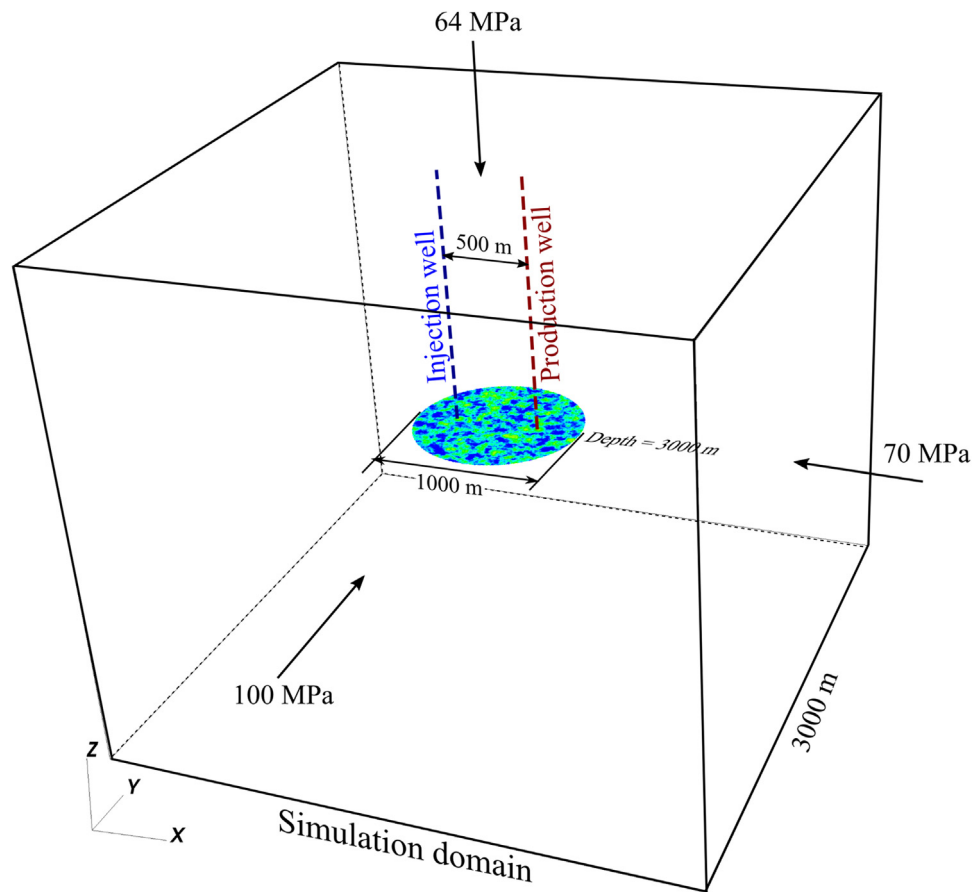


Fig. 2. A sketch of the numerical model showing the simulation domain dimensions, location and size of the fracture inside the host rock, the configuration of the two wells, and the in situ stress components. Color of the fracture plane denotes the aperture at a reference effective stress, with blue meaning smaller aperture and yellow wider. (For interpretation of the references to colour in this figure legend, the reader is referred to the web version of this article.)

the fracture depth, with a local vertical temperature gradient of $40^\circ\text{C}/\text{km}$.

Fluid flow in the system is assumed to be dominated by that along the fracture since the matrix permeability of typical EGS host rocks is extremely small. Leak-off from the fracture into the matrix and unsteady fluid flow within the matrix are naturally included in the simulations, since the numerical model essentially uses a porous medium formulation. However, their effects on the overall flow field and heat transport are expected to be negligible, and therefore the related results are not presented.

The dimensions of the simulation domain are approximately $3\text{ km} \times 3\text{ km} \times 3\text{ km}$, much larger than the volume affected by heat transfer, thereby sufficient for simulating the constraints of the far-field rock body in thermal stress development. The fracture is represented by a thin layer of elements $5\text{ m} \times 5\text{ m} \times 2\text{ mm}$ in size, and the dimensions of the rock matrix elements near the fracture are $5\text{ m} \times 5\text{ m} \times 5\text{ m}$ in size. The mesh becomes progressively coarser at locations farther from the fracture to reduce the computational cost. The computational domain consists of approximately 3,000,000 elements.

The downhole pressure in the production well at the depth of the fracture is kept at the initial pore pressure (34 MPa). At the injection well, water is injected at a constant temperature of 50°C (122°F) and a constant rate of 12.5 liter/second. This rate is considered reasonable from both engineering and economical perspectives (Baria et al., 1999; Bruel, 2002; Tenma et al., 2008; Jung, 2013; Pandey et al., 2014; Llanos et al., 2015; Hogarth and Bour, 2015). We apply a zero-flux boundary condition for flow and heat

transfer at the far-field boundaries. The thermo-mechanical solver applies the boundary condition of zero normal displacement on one boundary face in each direction and applies the specified *in situ* stress on the opposite boundary face in the same direction, which is a typical way of applying *in situ* stress while eliminating the rigid body motion of the simulation system.

The parameters for rock and fluid properties are listed in Table 1.

Note that the fluid dynamic viscosity value used is that of water under the reference temperature (200°C) and pressure (34 MPa) (Sengers and Kamgar-Parsi, 1984; Likhachev 2003). The dependency of fluid density on temperature and pressure is ignored in

Table 1
Rock properties, fluid properties, and other parameters used in the model.

Property name	Value
Porosity of the rock matrix (ϕ_m)	0.01
Permeability of the rock matrix (k_m)	$1 \times 10^{-20}\text{ m}^2$
Rock solid density (ρ_s)	$2,500\text{ kg/m}^3$
Rock bulk modulus (K)	33.3 GPa
Rock shear modulus (G)	20 GPa
Specific heat capacity of rock solid (C_s)	790 J/kg/K
Specific heat capacity of fluid (C_f)	$4.46 \times 10^3\text{ J/kg/K}$
Linear thermal expansion coefficient of rock matrix (α_r)	$8.0 \times 10^{-6}\text{ K}^{-1}$
Reference fluid density (ρ_f)	887.2 kg/m^3
Reference pressure for fluid density (P_f)	34 MPa
Reference temperature for fluid density (T_f)	200°C
Fluid dynamic viscosity (μ)	$1.42 \times 10^{-4}\text{ Pa}\cdot\text{s}$
Fluid compressibility (β_f)	$5.11 \times 10^{-10}\text{ Pa}^{-1}$
Volumetric thermal expansion coefficient of fluid (α_f)	$7.66 \times 10^{-4}\text{ K}^{-1}$
Thermal conductivity of rock matrix (K_m)	3.5 W/m/K

Table 2
Simulation plan of the aperture field.

	Mean (mm)	Standard deviation (mm)	Correlation length (m)	Number of realizations
Set 1: varying correlation length	0.24	0.17	12.5	20
	0.24	0.17	25	20
	0.24	0.17	50	20
	0.24	0.17	100	20
	0.24	0.17	200	20
Set 2: varying standard deviation	0.24	0.0425	12.5	10
	0.24	0.085	12.5	10
	0.24	0.17	12.5	10
	0.24	0.34	12.5	10
	0.24	0.68	12.5	10
	0.24	0.0425	200	20
	0.24	0.085	200	20
	0.24	0.17	200	20
	0.24	0.34	200	20
	0.24	0.68	200	20

the simulations, but the potential impact of this assumption is discussed in the concluding remarks.

3.2. Heterogeneous aperture fields

The aperture of a typical rock fracture can be statistically represented by a spatially autocorrelated random field (Tsang et al., 1988; Tsang and Tsang, 1989; Tsang and Neretnieks, 1998). In a given stress state, the apertures of a fracture had been found to typically follow the gamma distribution or the log-normal distribution (Tsang et al., 1988; Tsang and Tsang, 1989; Tsang and Neretnieks, 1998). The spatial autocorrelation characteristics are described by the variogram model and the correlation length λ . The variogram model describes how the semivariance, which is the statistical variance minus the covariance of the apertures, changes with the distance between any two locations. Three types of variogram models, namely the exponential, spherical, and Gaussian models are widely used in geostatistics (Cressie, 1993; Chiles and Delfiner, 2009) and normally the semivariance curves of these models do not significantly differ from each other when the correlation length is the same or when they are fitted to the same set of geostatistical data. We use the spherical variogram model for all the simulations conducted in this study. The variogram is assumed to be spatially isotropic on the fracture, with a nugget of zero. An intuitive interpretation of the correlation length is the distance beyond which the semivariance does not change significantly as the distance further increases. The three examples of aperture fields in Fig. 3 show that the sizes of the visible patches, within which the apertures do not significantly change, increase with greater correlation length. The λ/L ratio, with L being the characteristic flow length, is usually between 0.05 and 0.40 for typical hydrological applications (Tsang and Tsang, 1987, 1989; Moreno et al., 1988; Tsang et al., 1988).

In this study, the correlation length and standard deviation of the aperture values are the primary variables under investigation, as the spatial variation of apertures, not the mean aperture, determines the flow pattern and its evolution. Table 2 summarizes the plan for this investigation, in which simulation Set 1 is for the investigation of how the varying correlation length affects flow channeling and heat production, and simulation Set 2 is for the study of varying standard deviation of apertures. In Set 1, we adopt the aperture measurements in Tsang et al. (1988), and the apertures follow a log-normal distribution with a mean value of 0.24 mm and a standard deviation of 0.17 mm, which is denoted as log-normal (0.24 mm, 0.17 mm) hereafter. The selected correlation lengths covers a range of λ/L ratio from 0.025 to 0.4, with the characteristic flow length L being 500 m (the distance between the two wells). The effects of aperture's standard deviation on flow channeling may

depend on correlation lengths, so a sensitivity study of standard deviation is performed for the correlation lengths of 12.5 m and 200 m, and the values of standard deviation simulated is shown in Table 2.

To obtain statistically representative results requires a sufficiently large number of random realizations for each combination of the specified parameters. We use the frequentist method (Adcock, 1997) to determine the minimum number of realizations required in the study as

$$n_{\min} = \left(\frac{cs}{E} \right)^2 \quad (8),$$

where n_{\min} is the minimum realization number; c is the critical value, which is related to the probability that the variable lies in the specified confidence interval; s is the standard deviation of the desired variable; and E is the error of margin. Our analysis shows that the realization numbers listed in Table 2 are adequate for achieving a 90% probability that the production life lies in a confidence interval of ± 4 years ($E = 4.0$ years) with c being 1.645.

We use the “gstat” package in R, a programming language and software environment for statistical computing and graphics, to generate the aperture fields that follow the specified probability distribution and spatial autocorrelation in the initial state. The aperture fields are generated using the spherical variogram model with 20 cells nearby used for universal kriging. More detailed description of the “gstat” package for multivariable geostatistical modeling, prediction, and simulation, particularly the “vgm” function used in the current work for the generation of the aperture field, is available in Pebesma (2004). A disk-shaped proppant-enhanced aperture region, centered at the intersection between the fracture and each well, is superposed onto the aperture field (Fig. 3). This measure is to avoid the excessive pressure drop due to the high flow rate near the wells and it is also feasible in real world engineering. The proppant-enhancement of aperture is assumed to be 0.8 mm at the intersection point and linearly decreases to 0 mm when the radius reaches 50 m. The actual aperture used is the greater between the randomly generated aperture and the proppant-enhanced aperture.

As reasoned in Section 2.4, two constitutive parameters, a and b , are required to describe the relationship between the aperture and the effective stress at a fracture element. The constitutive behavior of a whole fracture would be described by the spatial distributions of a and b . However, what R directly generates is the spatial distribution of aperture under a given effective stress. To bridge this gap, we adopt the apertures A_{r1} and A_{r2} in two specified reference stress states $\sigma'_{n,r1}$ and $\sigma'_{n,r2}$ as an alternative set of independent parameters to describe the constitutive behavior of a fracture ele-

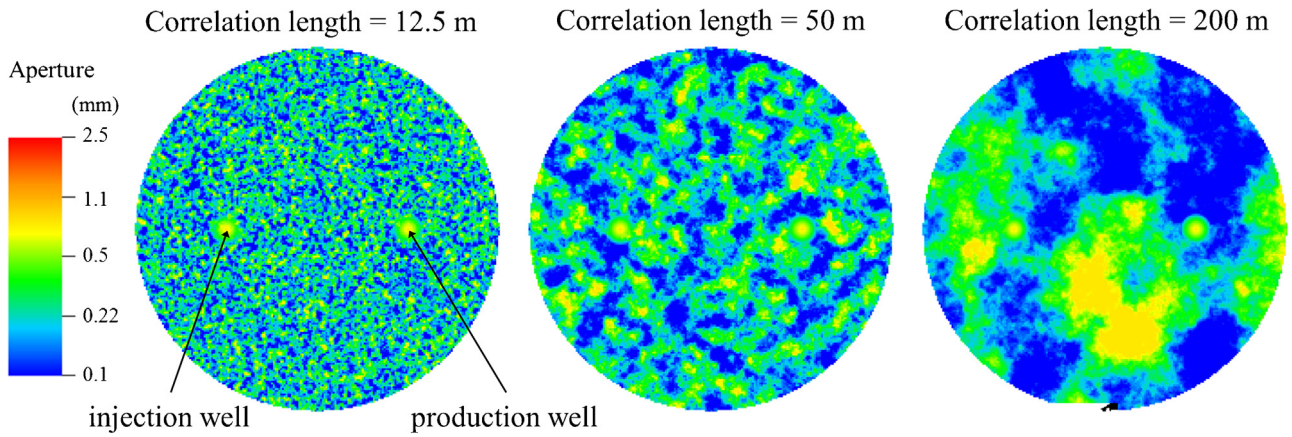


Fig. 3. Examples of aperture fields for the correlation lengths of 12.5 m, 50 m, and 200 m. The two small yellow disk-shaped areas in each aperture field are the proppant-enhanced regions centered at the intersection between the fracture and the injection and production wells. (For interpretation of the references to colour in this figure legend, the reader is referred to the web version of this article.)

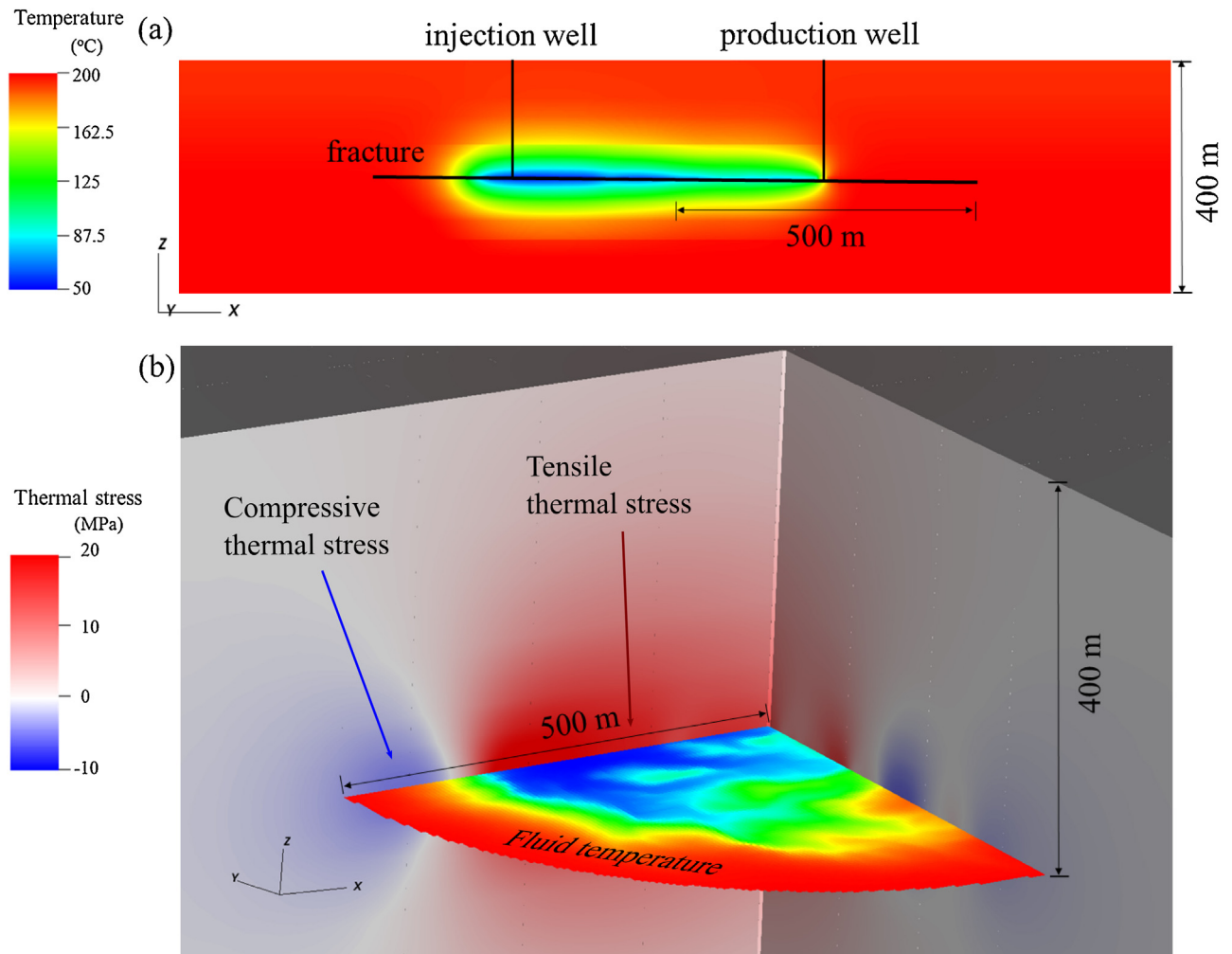


Fig. 4. Rock temperature and thermal stress after 30 years of production for a representative aperture field with log-normal(0.24 mm, 0.17 mm) and a correlation length of 50 m. (a) Temperature on a vertical cut along the plane of the two wells. (b) A 3D view of the thermal stress in the rock body and temperature distribution along the fracture. A quarter of the solid rock matrix is removed in (b) to show the internal structure of the stress field. The rock matrix farther than 400 m away from the fracture is not shown, although is included in the model. The fracture plane in this quarter is colored based on the fluid temperature using the same color map as that for (a). Note that tensile thermal stress is positive. (For interpretation of the references to colour in the text, the reader is referred to the web version of this article.)

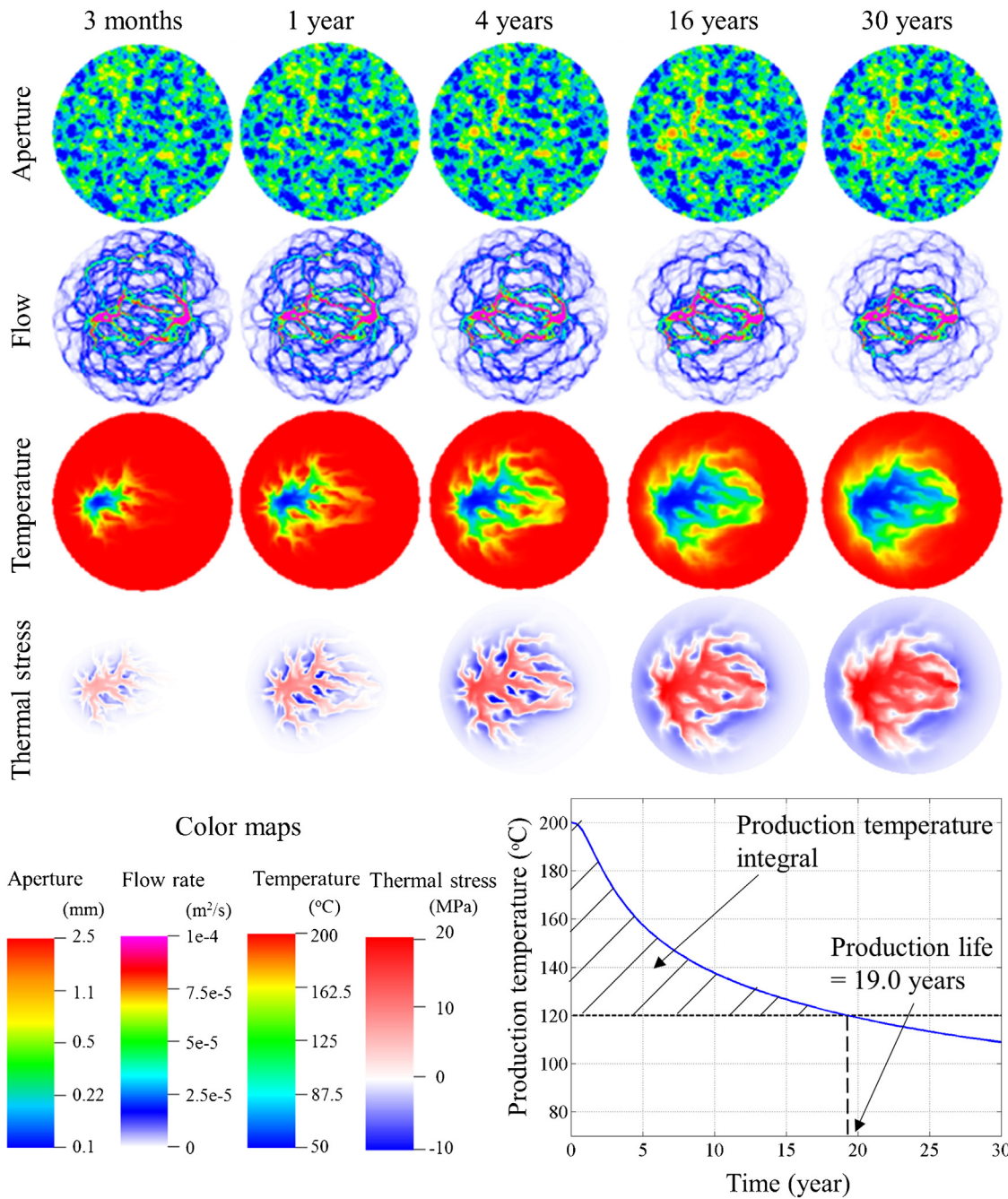


Fig. 5. Evolutions of aperture, flow, temperature, and thermal stress fields along the fracture, and production temperature curve for the example in Fig. 4. The same color maps are used in all the subsequent figures whenever applicable. Note that the aperture color map is in a logarithmic scale. The flow rate is the volume of fluid passing a unit-length cross section of the fracture per unit time, so the unit is m^2/s .

ment. The fields of A_{r1} and A_{r2} can be converted to the fields of a and b through the following relationships.

$$a = \frac{A_{r1}A_{r2}(A_{r2} - A_{r1})(\sigma_{r1} - \sigma_{r2})}{(\sigma_{r1}A_{r1} - \sigma_{r2}A_{r2})^2} \quad (9)$$

$$b = \frac{A_{r2} - A_{r1}}{\sigma_{r1}A_{r1} - \sigma_{r2}A_{r2}} \quad (10)$$

After switching to using A_{r1} and A_{r2} from using a and b as independent variables, each simulation requires two aperture fields corresponding to two given reference stress states to fully quantify the deformation characteristics of the fracture. We choose the

initial natural state (30 MPa effective normal stress) as the first reference state and use the aperture field generated following the design in Table 2 for this state. We choose the effective stress of 5 MPa as the second reference stress state and assume that the aperture in this state is three times of that in the first reference state. This seemingly arbitrary choice of the relationship between the apertures in these two states reflects the unfortunate lack of real data to support a more realistic model. However, it is sufficient for embodying the most essential behavior of rock joints concerned in this study: fracture aperture and permeability significantly increase as the effective stress decreases.

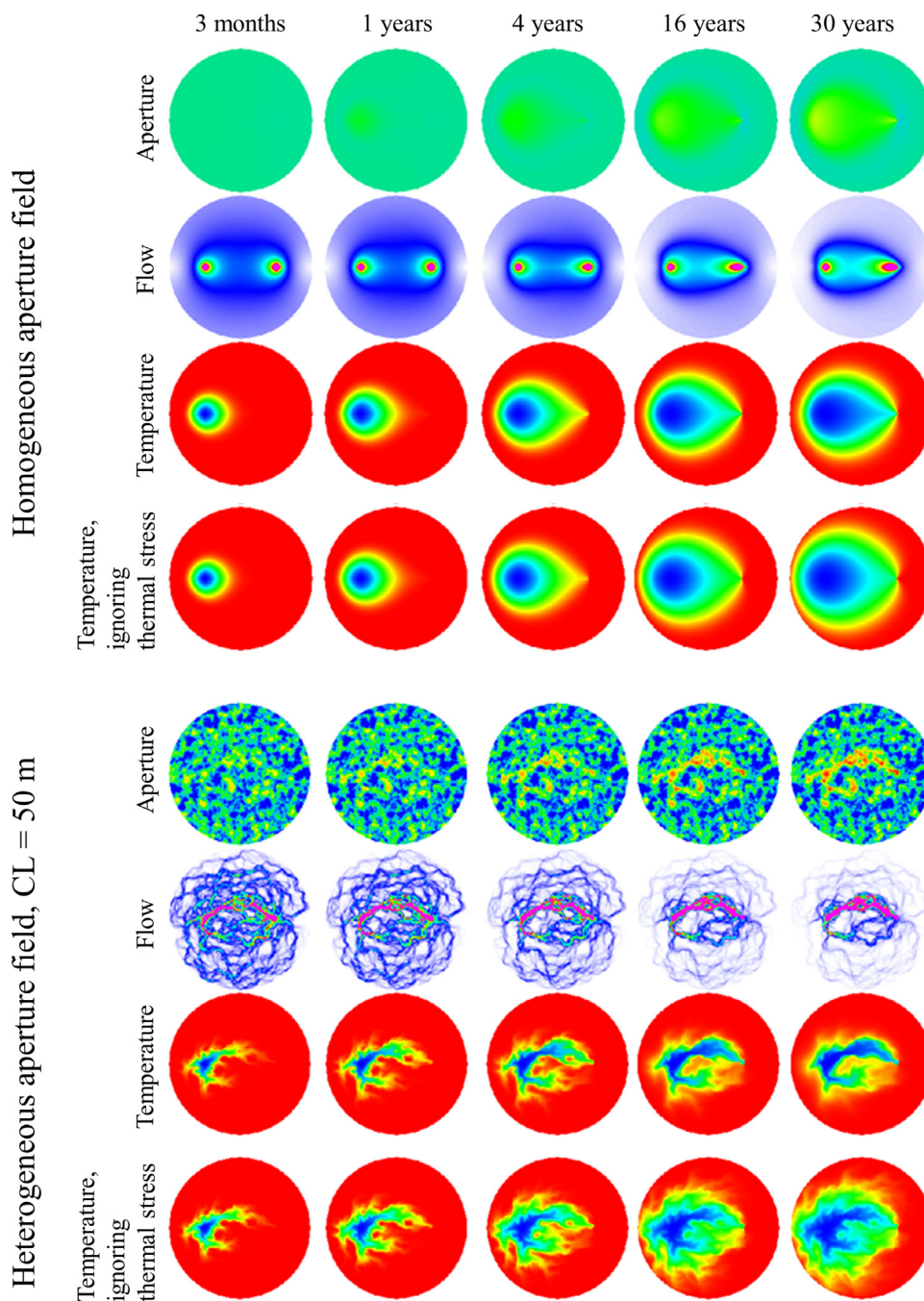


Fig. 6. Evolutions of aperture, flow, and temperature fields in a fracture with a homogeneous aperture field and a fracture with a heterogeneous aperture field from the full THM model, and the temperature field evolution from the reduced model that ignores the thermo-mechanical coupling. The aperture field and flow field do not significantly change when thermal stress is ignored, so they are not plotted for the reduced models.

The simulations were performed on LLNL's supercomputer Cab. A simulation for 30 years of heat production costs approximately 1,500 core-hours based on Intel® Xeon® E5-2670 processors. Thanks to GEOS's scalable parallel processing capability, each realization was simulated within 6h of wall time by 16 computing nodes (256 cores).

4. Simulation results

4.1. Results of one representative realization

This section uses the results of one representative simulation to illustrate the THM processes during EGS heat production and

to establish the paradigm for subsequent analyses. We analyze in detail the results for an aperture field with log-normal(0.24 mm, 0.17 mm) and a correlation length of 50 m. Fig. 4 shows the rock temperature and thermal stress in the rock body near the fracture after 30 years of production. The cooling front vertically advanced roughly 200 m in both sides of the fracture, as Fig. 4(a) shows, and the region with significant stress change reaches approximately 400 m away from the fracture plane in the vertical direction [Fig. 4(b)]. These observations reassures that a 3 km × 3 km × 3 km domain is sufficient for eliminating the boundary effect. Although the initial reservoir temperature has a vertical gradient, the region of temperature change is largely symmetric with respect to the fracture plane. This is because the heat conduction caused by the

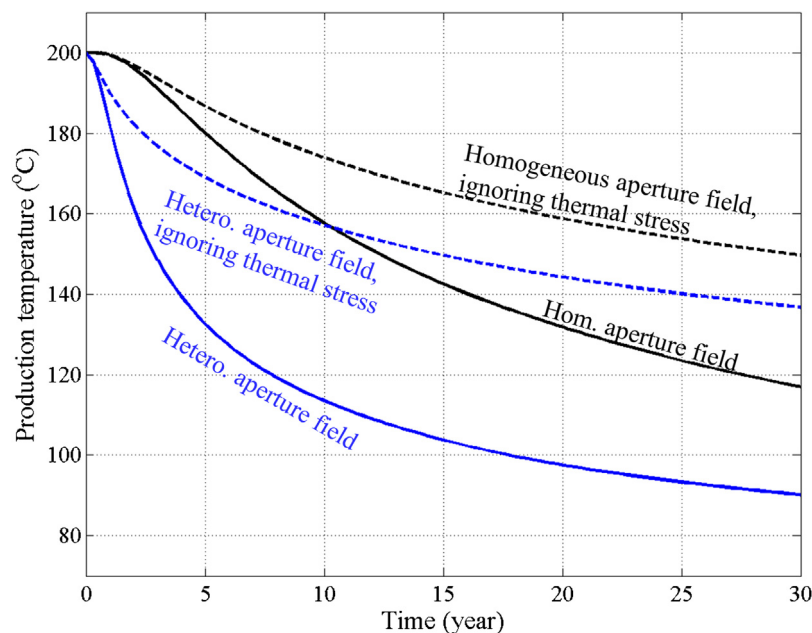


Fig. 7. Production temperature curves corresponding to the examples in Fig. 6.

Table 3

Statistical means and standard deviations of the production lives and production temperature integrals for different correlation lengths.

Correlation length (m)		12.5	25	50	100	200
Production life (year)	Mean	27.7	25	23.2	19.5	17.5
	Standard deviation	2.5	6.5	6.8	9.9	9.7
Production temperature integral ($^{\circ}\text{C} \times \text{year}$)	Mean	824	744	627	554	553
	Standard deviation	84	226	225	287	361

flow of cold water is much greater than that caused by the initial temperature gradient. The cooling of the rock body causes a tensile thermal stress (denoted by red color) in the cooled region, which reduces the compressive total vertical stress, shown in the 3D view of the thermal stress of the rock body in Fig. 4(b). We also notice that there exist some regions of increased compressive stress [blue color in Fig. 4(b)] around the tensile thermal stress region, which is caused by the redistribution of the vertical stress within the rock body. The compressive thermal stress reduces the aperture and flow rate outside the preferential paths, thus further exacerbates flow channeling.

Fig. 5 shows the evolutions of aperture, fluid flow rate, temperature, and thermal stress along the fracture, as well as the production temperature curve for the same example. The heterogeneous aperture field at the beginning of heat production causes unevenly distributed flow across the fracture, with a few preferential paths conducting a great portion of the fluid. As water circulation continues, the preferential paths become more apparent on both the aperture and flow fields. The rock body around the preferential paths cools faster than other portions and the shape of the horizontal cooling front follows the preferential paths. The region with tensile thermal stress on the fracture develops consistently with that of the cooling front. During this process, the production temperature continuously decreases following the thermal breakthrough as early as 3 months. This example evidently demonstrates that our THM numerical model captures the flow channeling mechanism described in Section 1 in a high fidelity.

To quantify the reservoir performance and make the subsequent statistical analysis of the hundreds of realizations tractable, we define the following two metrics of interest for EGS. (1) The production life is defined as the time period when the production temperature continuously decreases from the initial 200°C

to 120°C . The production life is counted as 30 years for statistical analysis if the production temperature remains above 120°C after 30 years of production. (2) The production temperature integral is defined as the area between the production temperature curve and the horizontal line of 120°C in a time–production temperature plot, as illustrated by the shaded area in the lower right corner of Fig. 5. This metric can quantify the useable heat produced by the EGS reservoir because of the same constant injection rate across all the simulations in this study.

4.2. Effects of thermal stress on flow channeling and heat production

In order to quantify the effects of thermal stress, we compare the results for the same initial aperture field using the full THM model and a reduced model in which the thermo-mechanical solver is disabled. The two models are applied to an idealized fracture with a spatially homogeneous aperture of 0.24 mm , denoted as the control case (not included in the simulation plan in Table 2), and a heterogeneous aperture field with log-normal(0.24 mm , 0.17 mm) and the correlation length of 50 m . Fig. 6 shows the evolutions of aperture, flow rate, and temperature fields for the homogeneous and heterogeneous aperture fields. If thermal stress is ignored, the aperture field and flow field do not change significantly during 30 years of production, so only the temperature fields for the reduced models are plotted. For either the homogeneous or heterogeneous aperture field, the area of the cooled zone is larger and the flow pattern is more diffuse in the reduced model than those in its full THM counterpart. The corresponding production temperature curves are plotted in Fig. 7. For the homogeneous aperture field, the production life considering the THM processes is 27.4 years and is greater than 30 years if thermal stress is ignored. The production temper-

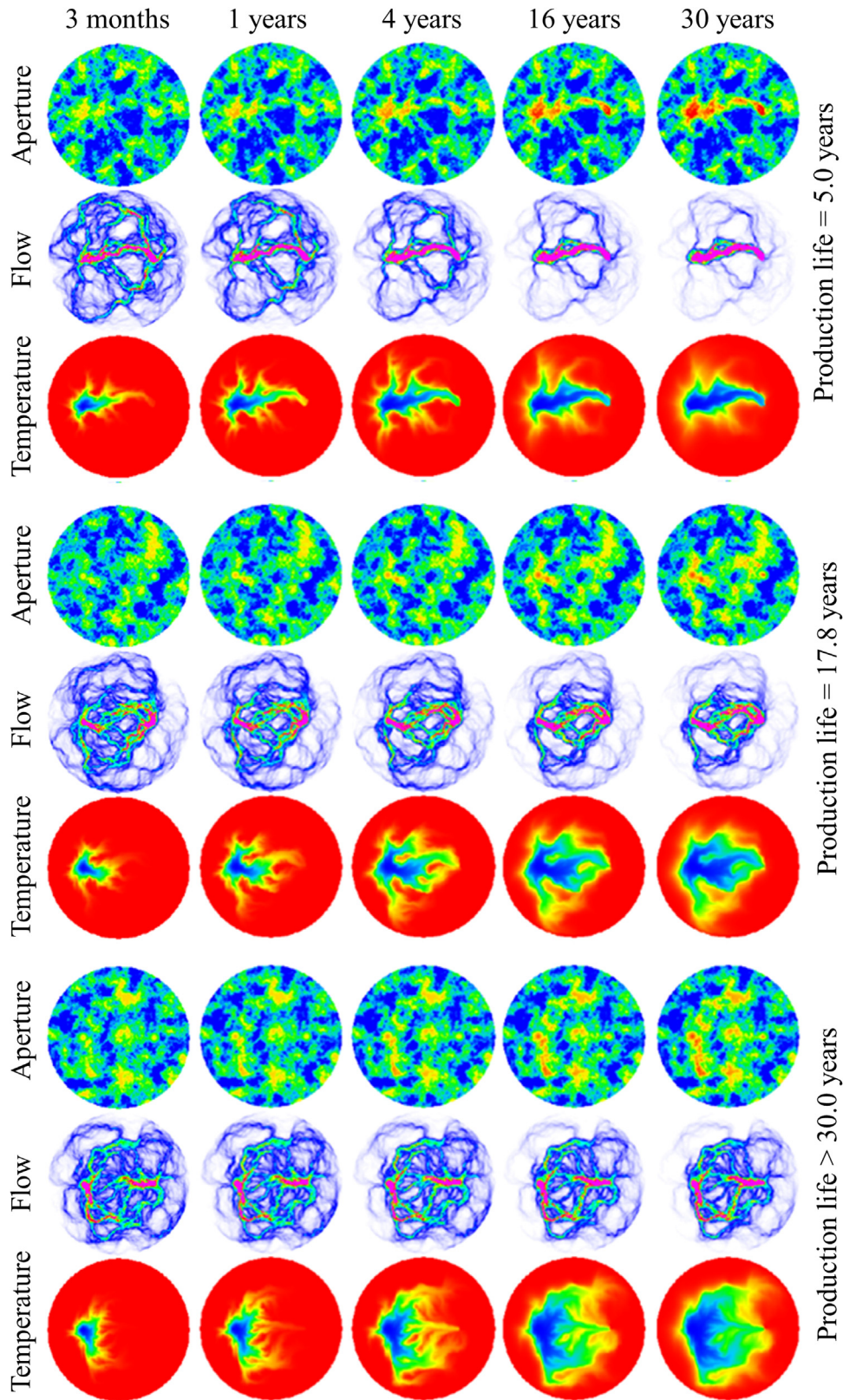


Fig. 8. Evolutions of aperture, flow, and temperature fields for three representative realizations, all with a correlation length of 100 m.

ature integral from the full THM model is approximately 60% of that from the reduced model. Thermal stress plays an even greater role in the case of heterogeneous aperture field. The production life considering the THM processes is 9.4 years, while it is longer than 30 years when the thermo-mechanical process is ignored;

the production temperature integral from the full THM model is only 28% of that from the reduced model. The results confirm that thermal stress plays a very important role in EGS production, and ignoring it can lead to remarkable overestimation of heat production.

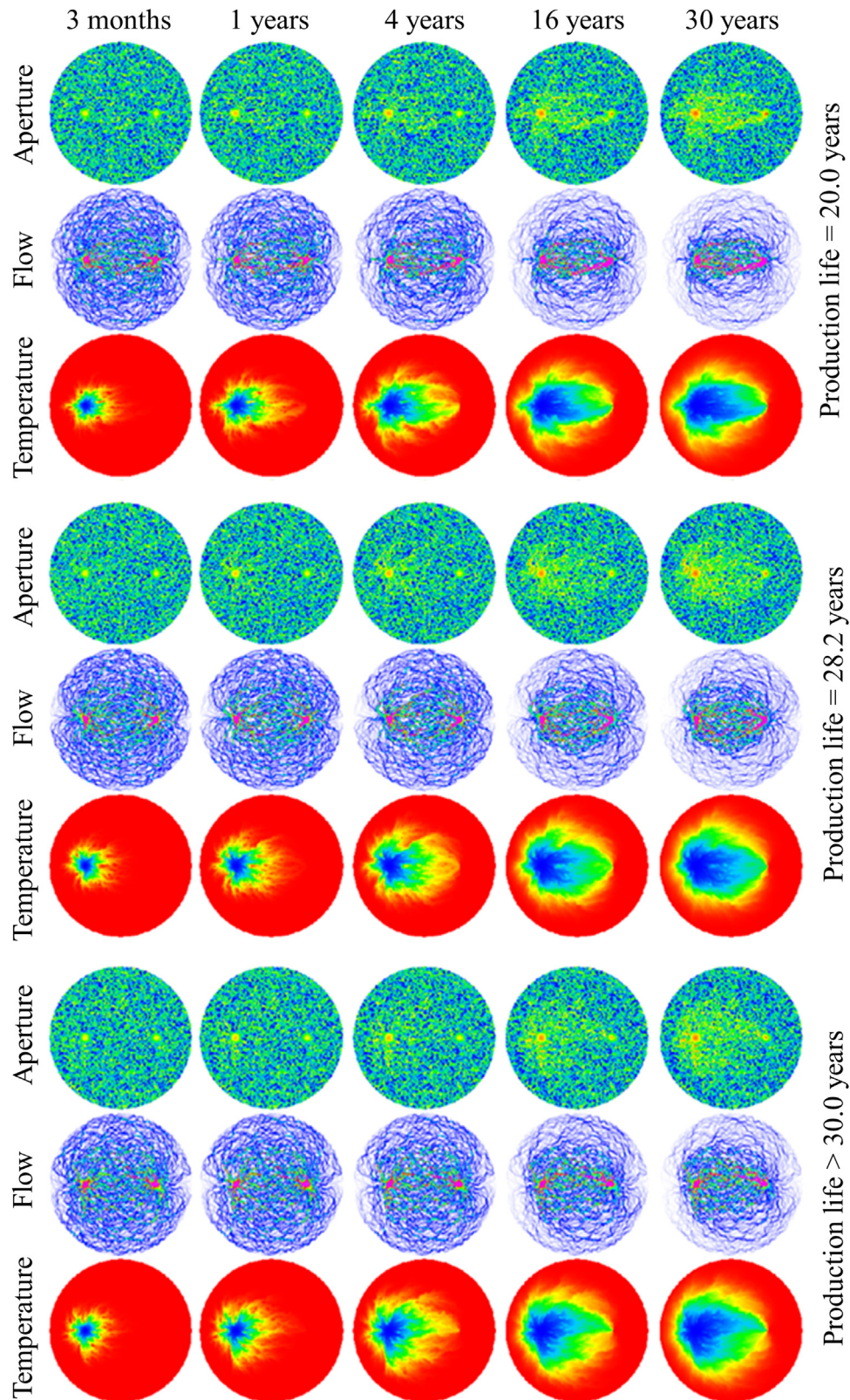


Fig. 9. Evolutions of aperture, flow, and temperature fields for representative realizations with the correlation length of 12.5 m.

4.3. Effects of correlation length on flow channeling and reservoir performance

Among the 20 realizations for each correlation length in simulation Set 1 (Table 2), we present the results of three representative

realizations for relatively short, medium, and long production lives, respectively. Fig. 8 shows the results for the correlation length of 100 m. In the first realization with a production life as short as 5.0 years, the initial aperture field enables a straight preferential path between the two wells, and the straight path becomes more and

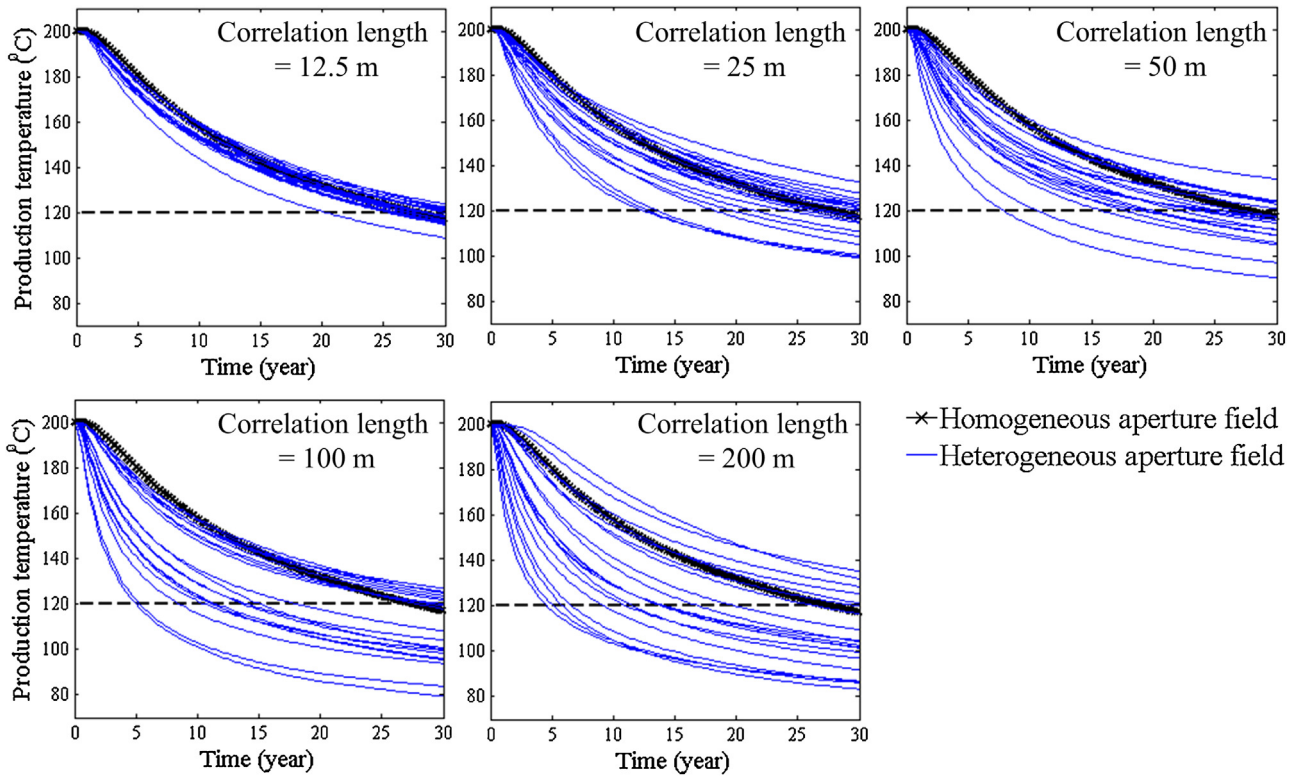


Fig. 10. Production temperature curves for all the realizations with log-normal(0.24 mm, 0.17 mm) and varying correlation length. The bold black curve in each sup-plot is based on the control case with homogeneous aperture field.

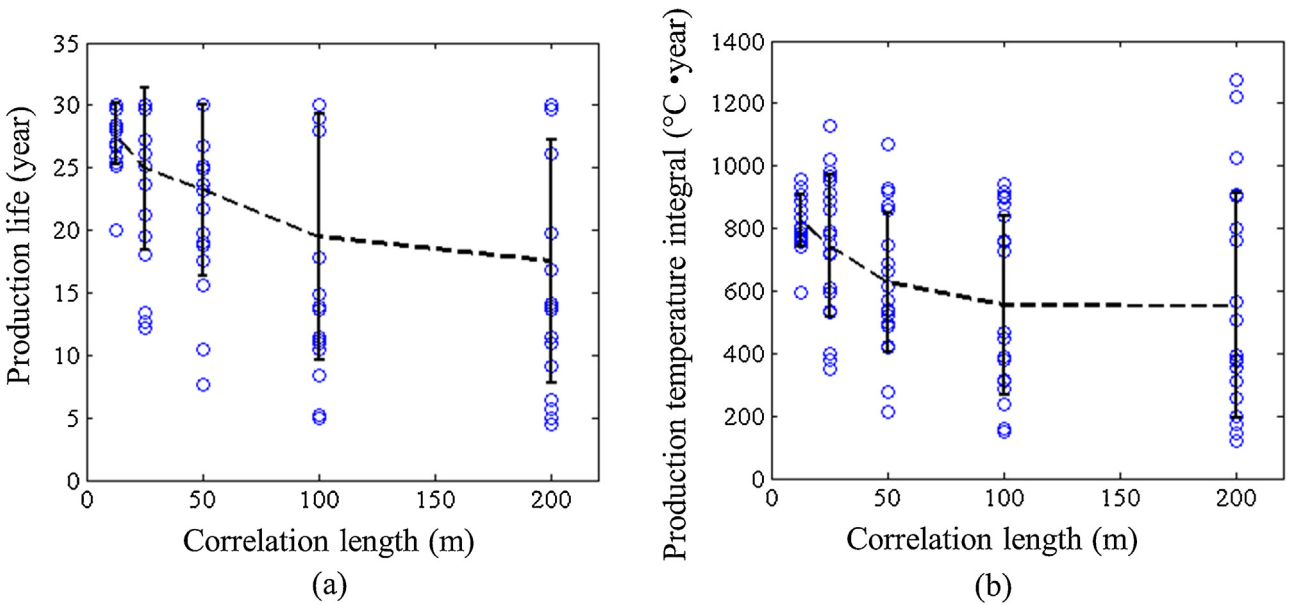


Fig. 11. Scatter plots of (a) production life and (b) production temperature integral marked with the means (dashed line) and standard deviations (error bars) for various correlation lengths.

more predominant during production. On the contrary, in the third realization the initial aperture field forces the development of multiple tortuous preferential paths by blocking the central region with a low transmissivity zone, leading to a more diffuse flow pattern and a production life beyond 30 years. The initial aperture field significantly affects the flow pattern evolution, as well as reservoir performance.

The representative results for the correlation length of 12.5 m are shown in Fig. 9. In contrast to the observations on the corre-

lation length of 100 m, the flow pattern shows limited variation among realizations and the range of the production life, i.e., from 20.0 years to beyond 30 years, is much narrower. Moreover, the evolutions of temperature fields in all the three examples resemble the temperature field evolution with the homogeneous aperture field (Fig. 6), which indicates that the fracture behaves similar to a homogeneous one when the correlation length is much shorter than the well distance of 500 m.

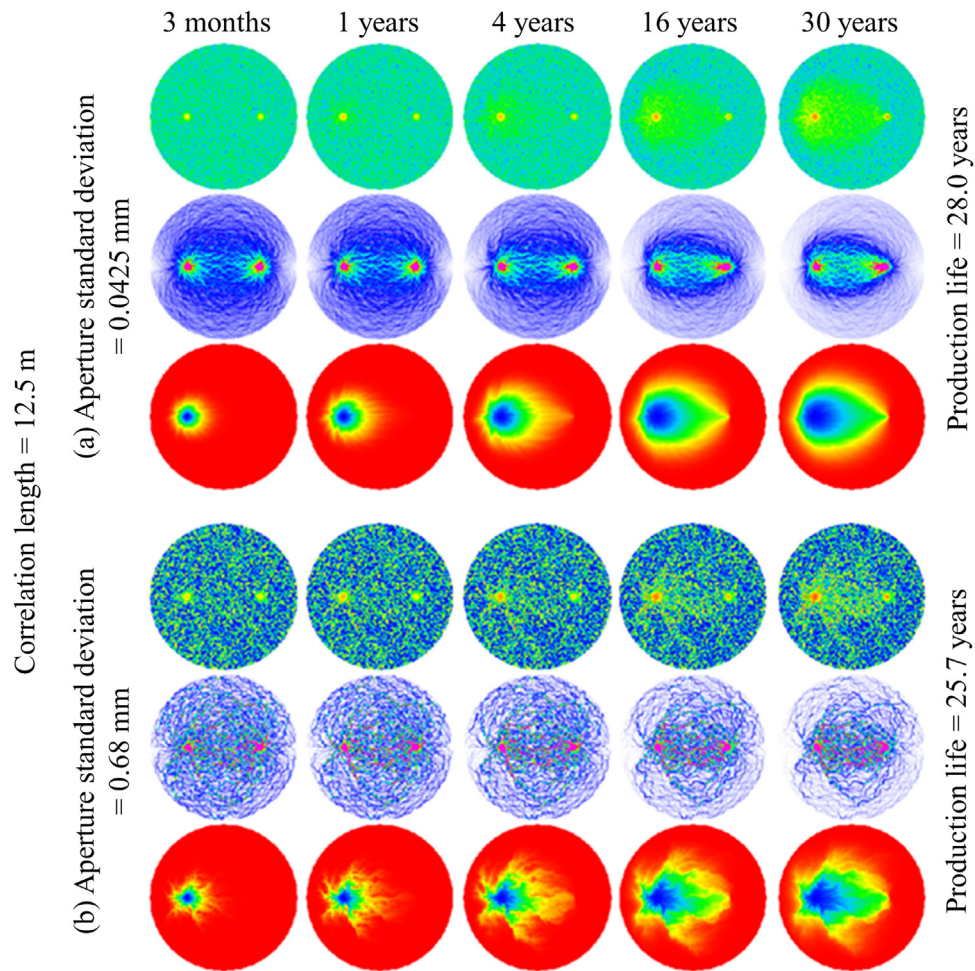


Fig. 12. Evolutions of aperture, flow, and temperature fields for a representative example of (a) the aperture field with log-normal(0.24 mm, 0.0425 mm) and the correlation length of 12.5 m, and (b) the aperture field with log-normal(0.24 mm, 0.68 mm) and the correlation length of 12.5 m.

Table 4
Statistical means and standard deviations of the production lives and production temperature integrals for different aperture standard deviations with the correlation length of 12.5 m and 200 m.

Correlation length = 12.5 m	Standard deviation (mm)		0.0425	0.085	0.17	0.34	0.68
			Production life (year)	Mean	28.3	27.7	27.1
Correlation length = 200 m	Production temperature integral (°C × year)	Standard deviation	1.4	1.8	3.4	2.4	3.5
		Mean	886	855	828	833	780
		Standard deviation	44	48	121	95	108
		Mean	23.7	22.7	17.4	15.2	12.6
Correlation length = 200 m	Production temperature integral (°C × year)	Standard deviation	5.1	7.7	9.2	9.1	9.3
		Mean	767	726	612	434	399
		Standard deviation	208	286	436	260	338
		Mean	208	286	436	260	338

Fig. 10 summarizes the production temperature curves for all the five correlation lengths with log-normal(0.24 mm, 0.17 mm), and the thick black curve on each subfigure is based on the control case with the homogeneous aperture field. The results show that the band comprising the production temperature curves becomes wider as the correlation length increases, which indicates the random variation of production temperature increases with longer correlation length. The production temperature curves are very similar to each other for correlation length = 12.5 m, which further confirms that a fracture with an aperture field of a small correlation length behaves similar to a fracture with a homogeneous aperture field. Besides, there are generally more production temperature curves below the curve for the control case than above it in each sub-plot, suggesting that the spatially heterogeneous aperture field generally tends to exacerbate flow channeling and cause inferior

reservoir performance. Occasionally, the heterogeneous aperture field may provide better reservoir performance than the homogeneous aperture field. In these cases, the flow fields are more diffuse than that in the control case when certain heterogeneous aperture fields force tortuous preferential paths and blocks the direct connection between the injection and production wells, as the third example in Fig. 8 shows.

Fig. 11 summarizes the production lives and production temperature integrals for various correlation lengths, and the statistical quantities are shown in Table 3. Both the mean production life and mean production temperature integral decrease with longer correlation length, and the standard deviations for both metrics generally increase with longer correlation length. These results are consistent with the observations in Fig. 10, thus are not further discussed here.

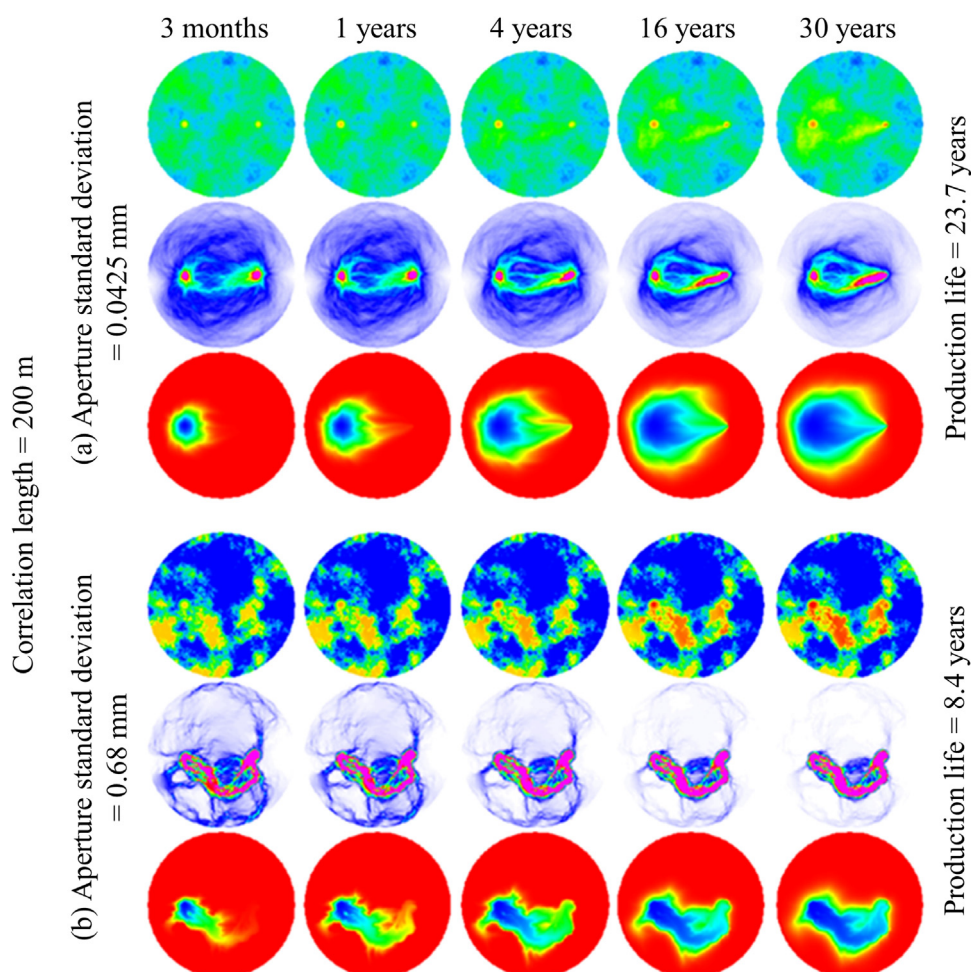


Fig. 13. Evolutions of aperture, flow, and temperature fields for a representative example of (a) the aperture field with log-normal(0.24 mm, 0.0425 mm) and the correlation length of 200 m, and (b) the aperture field with log-normal(0.24 mm, 0.68 mm) and the correlation length of 200 m.

4.3.1. Effects of aperture standard deviation

A number of realizations were simulated for various standard deviations of the aperture values and two correlation lengths (12.5 m and 200 m) as summarized in Table 2. Fig. 12 shows the results of two representative realizations of the correlation length of 12.5 m, with the smallest (0.0425 mm) and greatest (0.68 mm) standard deviations, respectively. Fig. 13 shows the results in the same manner for the correlation length of 200 m. For the correlation length of 12.5 m, although the flow channels are more distinct for greater aperture standard deviation, the evolutions of temperature field are only modestly affected by the aperture standard deviation (Fig. 12). This is because when the correlation length is short, the distance between the adjacent preferential paths is very small. The horizontal variation of rock temperature is significantly reduced by the heat conduction in the rock body. Therefore, the vertical propagation of the cooling front tends to resemble that with the homogeneous aperture field regardless of the aperture standard deviation. On the contrary, when the correlation length is 200 m, the aperture, flow, and temperature fields for the aperture field with the standard deviation of 0.68 mm evolve in profoundly different ways from those for the aperture field with the standard deviation of 0.0425 mm (Fig. 13). This is because the initial aperture field with greater standard deviation enables more distinct

preferential paths, and it is more likely to develop a dominant flow channel rather than multiple preferential paths.

The production lives and production temperature integrals for all the aperture standard deviations simulated and the correlation length of 12.5 m and 200 m are shown in Fig. 14, and the statistical quantities are listed in Table 4. When the correlation length is small, the reservoir performance only slightly changes with the change of aperture standard deviation. The production life and production temperature integral show overall decreasing trends as the standard deviation increases when the correlation length is long.

5. Concluding remarks

We developed a fully coupled thermo-hydro-mechanical (THM) numerical model to study the flow channeling process in a single fracture in engineered geothermal systems (EGS). Using this model, we studied the effects of spatial heterogeneity in a single fracture's aperture on flow pattern evolution and EGS heat production. The correlation length and standard deviation of the aperture field are the two primary variables under investigation, and hundreds of realizations were performed to ensure reservoir performance is statistically represented.

The simulation results show that thermal stress plays a very significant role in flow pattern evolution and heat production. Compared with homogeneous aperture fields, spatially heteroge-

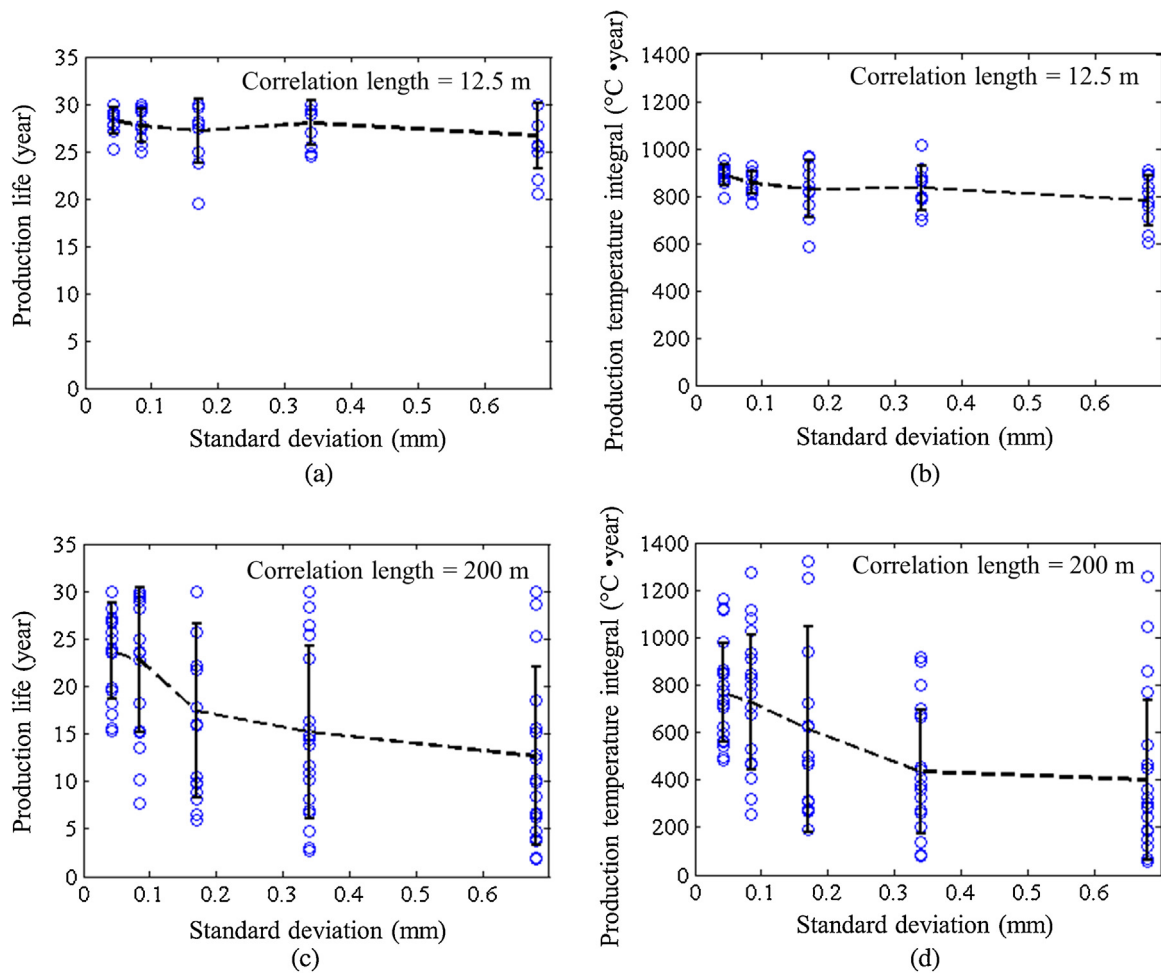


Fig. 14. Scatter plots of (a) production life and (b) production temperature integral for the correlation length of 12.5 m, and (c) production life and (d) production temperature integral for the correlation length of 200 m for various aperture standard deviations. The corresponding means are connected with dashed lines and the standard deviations denoted by error bars in each sub-plot.

neous aperture fields, which ubiquitously exist in nature, tend to exacerbate flow channeling and generally undermines reservoir performance. Flow channeling is inevitable regardless of the initial flow pattern, echoing the observations in Fu et al. (2015). However, post-thermal breakthrough temperature decline in the system studied in the current work is generally not as severe as that in the reservoir configuration studied in Fu et al. (2015). We discovered that a reservoir tends to have enduring heat production if the initial aperture field enables tortuous flow paths. When the aperture correlation length is much shorter than the characteristic flow length, the fracture behavior is similar to that of a homogeneous fracture. Longer correlation length generally leads to worse and more variable reservoir performance. The aperture standard deviation has little effect on heat production when the correlation length is relatively short, while it tends to reduce the amount of useful heat for long correlation lengths.

The aforementioned observations are consistent with intuitive reasoning of the role of aperture heterogeneity. Behavior of a heterogeneous fracture can approach that of an even fracture either by reducing the aperture standard deviation or by shortening the correlation length. On the other hand, our study provides important insights into fracture behavior as the aperture field deviates from a uniform aperture field by increasing the aperture standard deviation and/or correlation length.

We assumed constant water viscosity independent of temperature and pressure. Under the conditions concerned, water viscosity should increase with decreasing temperature and/or increasing pressure. This can, to some extent, impede the flow channeling process, as a hotter area of the fracture would have lower apparent impedance than a colder area with the same aperture. The current study ignored this effect to allow isolating the effects of aperture change caused by thermal stress. Although the reservoir performance has likely been slightly underestimated, the conclusions on the effects of aperture heterogeneity should remain similar to the above, had the temperature/pressure dependency of fluid viscosity been explicitly modeled.

The current study provides practically useful guidelines for developing sustainable EGS. The aperture field along a fracture is generally unknown *a priori*. Even after wells are drilled and circulation tests are performed, it is possible to infer only the mean aperture through hydraulic impedance interpretation. Quantifying the standard deviation and spatial autocorrelation characteristics of the aperture field remains extremely difficult, if possible at all. Therefore, making the injection and production wells far away from each other seems to be a simple and practical way to achieve a small ratio of the correlation length over the characteristic flow length. However, great well spacing could undermine inter-well hydraulic communication, which is problematic from a water

supply perspective. The present study found that under certain special circumstances, such as when direct inter-well flow paths are blocked by low transmissivity regions, heterogeneous aperture field may provide superb reservoir performance. A focus of our subsequent research is to identify well configurations that can reliably result in tortuous preferential paths.

Acknowledgements

The authors gratefully acknowledge the Geothermal Technologies Office of the U.S. Department of Energy for support of this work under the Enhanced Geothermal Systems Program. This work was performed under the auspices of the U.S. Department of Energy by Lawrence Livermore National Laboratory under Contract DE-AC52-07NA27344. We also acknowledge support from the National Science Foundation grant CBET-1133849 for Bin Guo through Princeton University. We gratefully acknowledge the many suggestions from Dr. Mark McClure that have substantially improved the quality of this paper. Release number: LLNL-JRNL-670552.

References

- Adcock, C., 1997. Sample size determination: a review. *J. R. Stat. Soc. Ser. D* 46 (2), 261–283.
- Ameli, P., Elkhoury, J.E., Morris, J.P., Detwiler, R.L., 2014. Fracture permeability alteration due to chemical and mechanical processes: a coupled high-resolution model. *Rock Mech. Rock Eng.* 47 (5), 1563–1573.
- Anderson, E.M., 1951. *The Dynamics of Faulting and Dyke Formation with Applications to Britain*. Hafner Pub. Co.
- Auradou, H., Drazer, G., Boschan, A., Hulin, J., Koplik, J., 2006. Flow channeling in a single fracture induced by shear displacement. *Geothermics* 35 (5), 576–588.
- Baisch, S., Vörös, R., Weidler, R., Wyborn, D., 2009. Investigation of fault mechanisms during geothermal reservoir stimulation experiments in the Cooper Basin, Australia. *Bull. Seismol. Soc. Am.* 99 (1), 148–158.
- Baisch, S., Weidler, R., Vörös, R., Wyborn, D., de Graaf, L., 2006. Induced seismicity during the stimulation of a geothermal HFR reservoir in the Cooper Basin, Australia. *Bull. Seismol. Soc. Am.* 96 (6), 2242–2256.
- Bandis, S.C., Lumsden, A.C., Barton, N.R., 1983. Fundamentals of rock joint deformation. *Int. J. Rock Mech. Min. Sci.* 20 (6), 249–268.
- Baria, R., Baumgärtner, J., Gérard, A., Jung, R., Garnish, J., 1999. European HDR research programme at Soultz-sous-forêts (France) 1987–1996. *Geothermics* 28 (4), 655–669.
- Barton, N., Bandis, S., Bakhtar, K., 1986. Strength, deformation and conductivity coupling of rock joints. *Int. J. Rock Mech. Min. Sci.* 22 (3), 121–140.
- Berkowitz, B., 2002. Characterizing flow and transport in fractured geological media: a review. *Adv. Water Resour.* 25 (8), 861–884.
- Bertani, R., 2012. Geothermal power generation in the world 2005–2010 update report. *Geothermics* 41, 1–29.
- Bower, K., Zyvoloski, G., 1997. A numerical model for thermo-hydro-mechanical coupling in fractured rock. *Int. J. Rock Mech. Min. Sci.* 34 (8), 1201–1211.
- Brown, D., 1997. Review of Fenton Hill HDR Test Results. No. LA-UR-97-434; CONF-970371-1. Los Alamos National Lab., NM (United States).
- Brown, D.W., 2009. Hot dry rock geothermal energy: important lessons from Fenton Hill. In: *Proceedings of the 34th Workshop on Geothermal Reservoir Engineering*. Stanford University, CA.
- Brown, D.W., Duchane, D.V., 1999. Scientific progress on the Fenton Hill HDR project since 1983. *Geothermics* 28 (4), 591–601.
- Bruel, D., 2002. Impact of induced thermal stresses during circulation tests in an engineered fractured geothermal reservoir: example of the Soultz-sous-forets European hot fractured rock geothermal project Rhine Graben, France. *Oil Gas Sci. Technol.* 57 (5), 459–470.
- Chiles, J., Delfiner, P., 2009. *Geostatistics: Modeling Spatial Uncertainty*. John Wiley & Sons.
- Chopra, P., Wyborn, D., 2003. Australia's first hot dry rock geothermal energy extraction project is up and running in granite beneath the Cooper Basin, NE South Australia. Proceedings of the Ishihara Symposium: Granites and Associated Metallogeneses, 43.
- Cook, N.G.W., 1992. Natural joints in rock: mechanical, hydraulic and seismic behaviour and properties under normal stress. *Int. J. Rock Mech. Min. Sci.* 29 (3), 198–223.
- Cook, R.D., Malkus, D.S., Plesha, M.E., Witt, R.J., 2007. *Concepts and Applications of Finite Element Analysis*. John Wiley & Sons.
- Cressie, N., 1993. *Statistics for spatial data*. Wiley series in probability and statistics.
- Danko, G., Bahrami, D., 2012. A new THMC model development for discrete-fracture EGS studies. *Geotherm. Resour. Council*.
- Deng, H., Fitts, J.P., Crandall, D., McIntyre, D., Peters, C.A., 2015. Alterations of fractures in carbonate rocks by CO₂-acidified brines. *Environ. Sci. Technol.* 49 (16), 10226–10234.
- Fu, P., Carrigan C.R., 2012. Modeling responses of naturally fractured geothermal reservoir to low-pressure stimulation. The 36th annual meeting of geothermal resources council 36: 429–433.
- Fu, P., Johnson, S.M., Carrigan, C.R., 2013. An explicitly coupled hydro-geomechanical model for simulating hydraulic fracturing in arbitrary discrete fracture networks. *Int. J. Numer. Anal. Methods Geomech.* 37 (14), 2278–2300.
- Fu, P., Hao, Y., Walsh, S.D.C., Carrigan, C.R., 2015. Thermal drawdown-induced flow channeling in fractured geothermal reservoirs. *Rock Mech. Rock Eng.*, <http://dx.doi.org/10.1007/s00603-015-0776-0>.
- Gener, A., Cuenot, N., Goerke, X., Bernd, M., Sanjuan, B., Scheiber, J., 2012. Status of the Soultz geothermal project during exploitation between 2010 and 2012. In: *Proceedings of the 37th Workshop on Geothermal Reservoir Engineering*. Stanford University, CA.
- Gener, A., Cuenot, N., Melchert, B., Moeckes, W., Ravier, G., Sanjuan, B., Sanjuan, R., Scheiber, J., Schill, E., Schmittbuhl, J., 2013. Main achievements from the multi-well EGS Soultz project during geothermal exploitation from 2010 and 2012. *Proceedings European Geothermal Congress*.
- Guo, B., Fu, P., Hao, Y., Carrigan, C.R., 2015. Thermal drawdown-induced flow channeling in a single heterogeneous fracture in geothermal reservoir. In: *Proceedings of the 40th workshop on geothermal reservoir engineering*. Stanford University, CA.
- Hayashi, K., Willis-Richards, J., Hopkirk, R.J., Niibori, Y., 1999. Numerical models of HDR geothermal reservoirs—a review of current thinking and progress. *Geothermics* 28 (4), 507–518.
- Hicks, T.W., Pine, R.J., Willis-Richards, J., Xu, S., Jupe, A.J., Rodrigues, N.E.V., 1996. A hydro-thermo-mechanical numerical model for HDR geothermal reservoir evaluation. *Int. J. Rock Mech. Min. Sci.* 33 (5), 499–511.
- Hogarth, R.A., Bour, D., 2015. Flow performance of the Habanero EGS closed loop. *Proceedings World Geothermal Congress, Melbourne, Australia*.
- Jung, R., 2013. EGS—Goodbye or back to the future. *Effective and Sustainable Hydraulic Fracturing*: 95–121.
- Koh, J., Roshan, H., Rahman, S.S., 2011. A numerical study on the long term thermo-poroelastic effects of cold water injection into naturally fractured geothermal reservoirs. *Comput. Geotech.* 38 (5), 669–682.
- Kohl, T., Evansi, K., Hopkirk, R., Rybach, L., 1995. Coupled hydraulic, thermal and mechanical considerations for the simulation of hot dry rock reservoirs. *Geothermics* 24 (3), 345–359.
- Kolditz, O., Clauser, C., 1998. Numerical simulation of flow and heat transfer in fractured crystalline rocks: application to the hot dry rock site in Rosemanowes (UK). *Geothermics* 27 (1), 1–23.
- Kosakowski, G., Berkowitz, B., Scher, H., 2001. Analysis of field observations of tracer transport in a fractured till. *J. Contam. Hydrol.* 47 (1), 29–51.
- Likhachev, E., 2003. Dependence of water viscosity on temperature and pressure. *Tech. Phys.* 48 (4), 514–515.
- Llanos, E.M., Zarrouk, S.J., Hogarth, R.A., 2015. Numerical model of the Habanero geothermal reservoir, Australia. *Geothermics* 53, 308–319.
- Lund, J.W., Freeston, D.H., Boyd, T.L., 2011. Direct utilization of geothermal energy 2010 worldwide review. *Geothermics* 40 (3), 159–180.
- McClure, M.W., Horne, R.N., 2014. An investigation of stimulation mechanisms in enhanced geothermal systems. *Int. J. Rock Mech. Min. Sci.* 72, 242–260.
- McDermott, C.I., Randriamanjatoa, A.R., Tenzer, H., Kolditz, O., 2006. Simulation of heat extraction from crystalline rocks: the influence of coupled processes on differential reservoir cooling. *Geothermics* 35 (3), 321–344.
- Méheust, Y., Schmittbuhl, J., 2000. Flow enhancement of a rough fracture. *Geophys. Res. Lett.* 27 (18), 2989–2992.
- Moreno, L., Tsang, Y., Tsang, C., Hale, F., Neretnieks, I., 1988. Flow and tracer transport in a single fracture: A stochastic model and its relation to some field observations. *Water Resour. Res.* 24 (12), 2033–2048.
- Neretnieks, I., 1987. Channeling effects in flow and transport in fractured rocks—some recent observations and models. *Proceedings of GEOVAL-87, International Symposium, Stockholm, Sweden*, 315.
- Pandey, S., Chaudhuri, A., Kelkar, S., Sandeep, V., Rajaram, H., 2014. Investigation of permeability alteration of fractured limestone reservoir due to geothermal heat extraction using three-dimensional thermo-hydro-chemical (THC) model. *Geothermics* 51, 46–62.
- Parker, R., 1999. The Rosemanowes HDR project 1983–1991. *Geothermics* 28 (4), 603–615.
- Pebesma, E.J., 2004. Multivariable geostatistics in S: the gstat package. *Comput. Geosci.* 30 (7), 683–691.
- Pruess, K., 1990. Modeling of geothermal reservoirs: fundamental processes, computer simulation and field applications. *Geothermics* 19 (1), 3–15.
- Sengers, J., Kamgar-Parsi, B., 1984. Representative equations for the viscosity of water substance. *J. Phys. Chem. Ref. Data* 13 (1), 185–205.
- Settgast, R., Johnson, S., Fu, P., Walsh, S.D.C., Ryerson, F., 2012. Simulation of hydraulic fracture networks in three dimensions. In: *Proceedings of the 37th workshop on geothermal reservoir engineering*. Stanford University, CA.
- Taron, J., Elsworth, D., 2009. Thermal-hydrologic-mechanical-chemical processes in the evolution of engineered geothermal reservoirs. *Int. J. Rock Mech. Min. Sci.* 46 (5), 855–864.
- Tenma, N., Yamaguchi, T., Zyvoloski, G., 2008. The Hijiori hot dry rock test site, Japan: Evaluation and optimization of heat extraction from a two-layered reservoir. *Geothermics* 37 (1), 19–52.
- Tester, J.W., Anderson, B.J., Batchelor, A., Blackwell, D., DiPippo, R., Drake, E., Garnish, J., Livesay, B., Moore, M., Nichols, K., 2006. The future of geothermal energy. In: *Impact of Enhanced Geothermal Systems (EGS) on the United*

- States in the 21st Century. Massachusetts Institute of Technology, Cambridge, MA, pp. 372.
- Tsang, C., Neretnieks, I., 1998. Flow channeling in heterogeneous fractured rocks. *Rev. Geophys.* 36 (2), 275–298.
- Tsang, Y.W., Tsang, C., 1987. Channel model of flow through fractured media. *Water Resour. Res.* 23 (3), 467–479.
- Tsang, Y., Tsang, C., 1989. Flow channeling in a single fracture as a two-dimensional strongly heterogeneous permeable medium. *Water Resour. Res.* 25 (9), 2076–2080.
- Tsang, Y., Tsang, C., Neretnieks, I., Moreno, L., 1988. Flow and tracer transport in fractured media: a variable aperture channel model and its properties. *Water Resour. Res.* 24 (12), 2049–2060.